

Modern potentials and the properties of condensed ^4He

M. H. Kalos, Michael A. Lee, and P. A. Whitlock

Courant Institute of Mathematical Sciences, New York University, 251 Mercer Street, New York, New York, 10012

G. V. Chester

Laboratory of Atomic and Solid State Physics, Cornell University, Ithaca, New York 14853

(Received 19 January 1981)

The Green's-function Monte Carlo method has been used to calculate the properties of the ground-state ^4He with several modern potentials. One potential, dubbed HFDHE2, by Aziz *et al.*, gave very good agreement with the experimental equation of state in both the liquid and crystal phases. Other properties such as the structure factor and the momentum distribution also compare well with the experiment. In both phases, perturbative estimates of the three-body Axilrod-Teller potential were computed. When they are added to the two-body energies, the total energy is no longer in agreement with experiment. Further investigation on the nature of three-body interactions in the ^4He may be necessary to elucidate this problem.

I. INTRODUCTION

Traditionally, the properties of simple fluids have been described by assuming that the dominant interactions in the system are two-body forces. As more information accumulates from experiments sensitive to pair interactions, theorists attempt to find potentials which best explain the results, and then use such potentials in calculations. Agreement with experiments on dense systems usually improves when three-body interactions are also included in the calculations. Estimates of the importance of higher order terms¹ in the potential suggest that they are minor in comparison with the two-body terms for systems such as liquid argon or liquid helium. We have been following this approach in investigating simple fluids and report here our calculations using modern two-body potentials for ^4He .

The most popular two-body potential used in theoretical studies of ^4He is the Lennard-Jones (LJ) 6-12 potential

$$V(r) = 4\epsilon \left[\left(\frac{\sigma}{r} \right)^{12} - \left(\frac{\sigma}{r} \right)^6 \right], \quad (1.1)$$

$$\epsilon = 10.22 \text{ K}, \quad \sigma = 2.556 \text{ \AA},$$

with parameters determined by de Boer and Michels² from second virial coefficients. Variational calculations³ on liquid ^4He which used the LJ potential have failed to reproduce accurately the energy or other measured properties of the real system. This was attributed partly to the inadequacies in the LJ potential and partly to deficiencies in the Jastrow wave function, a product of two-body correlation factors, used in the calculation. However, when other potentials

were used in variational studies,^{3(b),4} none gave a great improvement in the results. Recent work⁵ has shown that the major shortcoming of the Jastrow wave function is its omission of significant three-body correlations. A reconsideration of the two-body potential remains to be done.

Since the work of de Boers and Michels, much more experimental two-body data have been gathered. The new information has been employed to fit new He-He potentials and also to test how well other potentials can predict experimental measurements. For example, Jody and co-workers⁶ compared the prediction of seven different semiempirical potentials with thermal conductivity data. The comparison indicated that LJ was the least realistic of the seven in the repulsive core of the potential. Crossed molecular beam experiments⁷ have probed the attractive region of the potential and have determined that the position of the energy minimum r_m is $2.97 \pm 0.1 \text{ \AA}$ with a well depth of $10.7 \pm 0.4 \text{ K}$. Accurate *ab initio* calculations⁸ of the He-He potential indicate that the minimum energy is $10.8 \pm 0.1 \text{ K}$. These results confirm that LJ with well depth of 10.22 K and r_m of 2.87 \AA is not the best potential to use in describing the interaction of two helium atoms.

The best two-body helium potential for the gas phase and the effective two-body potential in a dense many-body system need not be the same. For example, the Lennard-Jones (12-6) potential for argon fitted to high-temperature second virial coefficients does not describe all of the properties of liquid or solid argon; and in fact, it does not fit low-temperature second virial coefficients.^{1(a),9} Recently the properties of liquid and solid ^4He were simulated exactly.¹⁰ The calculations used the Green's-function Monte Carlo (GFMC) method^{10,11} to solve the

Schrödinger equation with results subject only to statistical sampling errors and to small size corrections. A striking conclusion of that paper was that the LJ potential could describe a many-body ${}^4\text{He}$ system reasonably well. The remaining discrepancies between the simulation results and experiment can be attributed to the potential. We have recently embarked upon a survey of some alternative potentials to LJ. Our strategy was to predict to first order the value of the energy in the many-body system when another potential was used by employing Rayleigh-Schrödinger (RS) perturbation theory. That is, we perturbed our LJ GFMC energies and used the radial distribution function from our LJ results to calculate corrections to the energy. First-order perturbation theory has been shown by further GFMC calculations to be an excellent tool in investigating the effects of other potentials, as will be documented below.

II. ALTERNATIVE POTENTIALS

Based on the results of our survey using perturbation theory we chose three potentials with which to perform GFMC simulations. One potential, the ESMMSV potential of Burgmans and co-workers,^{7(b)} was fitted to their elastic differential collision cross sections for ${}^4\text{He}$ - ${}^3\text{He}$. The repulsive part of the potential was derived from backward glory scattering data and dispersion coefficients were obtained from theory. The data were fitted to a piecewise exponential spline-Morse-Morse-spline-van der Waals form for the potential. The other two potentials, MS12G6 and HFDHE2, were proposed in a recent paper by Aziz *et al.*¹² The MS12G6 potential is a modification of the generalized Lennard-Jones potential suggested by Maitland and Smith,¹³

$$V(r) = \epsilon \left[\left(\frac{6}{n-6} \right) \left(\frac{r_m}{r} \right)^n - \left(\frac{n}{n-6} \right) \left(\frac{r_m}{r} \right)^6 \right], \quad (2.1)$$

where the new parameters are

$$\epsilon = 10.9 \text{ K}, \quad n = 12 + 6 \left[\frac{r}{r_m} - 1 \right], \quad r_m = 2.967 \text{ \AA}.$$

The parameters ϵ and r_m , were determined by fitting the potential to high-temperature viscosity data, second virial data, and thermal conductivity data. The HFDHE2 potential is derived from a potential form proposed by Ahlrichs *et al.*,¹⁴

$$V(r) = \epsilon \left\{ A \exp \left[\frac{-\alpha r}{r_m} \right] - \left[C_6 \left(\frac{r_m}{r} \right)^6 + C_8 \left(\frac{r_m}{r} \right)^8 + C_{10} \left(\frac{r_m}{r} \right)^{10} \right] F(r) \right\}, \quad (2.2)$$

where

$$F(r) = \begin{cases} \exp \left[- \left(\frac{Dr_m}{r} - 1 \right)^2 \right], & \frac{r}{r_m} \leq D \\ 1, & \frac{r}{r_m} > D \end{cases}.$$

Aziz *et al.* fitted the potential to the self-consistent-field Hartree-Fock (SCFHF) calculations of McLaughlin and Schaefer¹⁵ restricted to the range 4.0–5.0 a.u., to second virial data, and to thermal conductivity data. The dispersion coefficients were modified within the bounds given by Tang *et al.*¹⁶ The values of the parameters for the HFDHE2 potential as reported by Aziz *et al.* are

$$\begin{aligned} A &= 0.5448504 \times 10^6 & \epsilon/\kappa &= 10.8 \text{ K} \\ \alpha &= 13.353384 & C_6 &= 1.37732412 \\ D &= 1.241314 & C_8 &= 0.4253785 \\ r_m &= 2.9673 \text{ \AA} & C_{10} &= 0.178100 \end{aligned}$$

Aziz *et al.* compared the predictions of these potentials and several others with a large accumulation of experimental two-body measurements. They conclude that the HFDHE2 potential gives the best overall agreement with experiment. The MS12G6 potential compared almost as well as HFDHE2 and ESMMSV gave an acceptable agreement; none of the potentials agreed with all the experimental data.

Our initial GFMC calculations indicated that the HFDHE2 potential gives excellent values for the energy of a many-body system. We therefore used the HFDHE2 potential to calculate the equation state of liquid and solid ${}^4\text{He}$. Our work with LJ ${}^4\text{He}$ showed that we cannot distinguish between the fcc and hcp phases in the ground state, so we again studied the fcc phase. We conclude that the HFDHE2 potential gives a very good account of the properties of condensed ${}^4\text{He}$. Furthermore, our calculations show that the ESMMSV and the MS12G6 potentials are unsatisfactory when used in a many-body system.

In the following section, a brief review of the GFMC method is given. We shall discuss how we obtained the wave functions we used to initiate our Monte Carlo iterations and give a description of simple perturbation theory. Section IV will contain the results of our calculations for both the liquid and crystal states.

III. METHODS

The simulations of the many-body ${}^4\text{He}$ system with HFDHE2 pair potentials were carried out by using the Green's-function Monte Carlo method. In this method, the Schrödinger equation is transformed into an integral equation by a Green's function for the Hamiltonian with a shifted energy scale. The integral equation is solved by a Neumann series, and the

iterations are carried out by Monte Carlo. A detailed description of the technique is given in Ceperley and Kalos^{11(a)} and Kalos, Levesque, and Verlet (KLV).^{11(b)} A thorough discussion of errors and the application of the method to the LJ ⁴He is given in Whitlock, Ceperley, Chester, and Kalos (WCKK)^{10(b)} and Whitlock, Kalos, Chester, and Ceperley (WKCC).^{10(a)}

The iteration of the Neumann series to solve the integral equation is initiated with a trial wave function $\psi^{(0)}(R)$, R being a point in configuration space. In our calculations we have chosen a trial wave function of the Jastrow form

$$\psi^{(0)}(R) = \exp\left[-\frac{1}{2} \sum_{i < j} u(r_{ij})\right]. \quad (3.1)$$

Since the trial wave function is used to accelerate the convergence of the GFMC iterations, as well as initiate the iterations, we tried to use pseudopotentials, u , which are optimal for the HFDHE2 potential. We took the results of functional optimizations of the Jastrow wave function by the paired phonon-analysis (PPA) method as described by Pinski and Campbell.¹⁷ In this method, one solves the extremum condition

$$0 = \frac{\partial}{\partial u(r)} \frac{\langle \psi_J | H | \psi_J \rangle}{\langle \psi_J | \psi_J \rangle} \quad (3.2)$$

to find the best variational $u(r)$. Equation (3.2) can be rewritten as an integrodifferential equation in terms of the radial distribution function, $g(x)$; the pair-pair correlation function, $P(\bar{x}, \bar{y}) = 2\rho\delta g(\bar{y})/\delta u(\bar{x})$, and the interaction potential, $V(r)$. The extremum condition is solved by a predictor-corrector procedure.¹⁸ The hypernetted-chain approximation (HNC) is used to approximate $g(x)$ and integrals containing $P(\bar{x}, \bar{y})$.

Pseudopotentials generated in this manner were used in the GFMC calculations for liquid densities with the HFDHE2, ESMMSV, and MS12G6 poten-

tials. The rate at which the GFMC calculation converges to the final energy suggests that the $u(r)$ obtained from the paired phonon analysis are very good. Also, the small degree of extrapolation (cf. WCKK) needed to extract exact properties such as $g(r)$ and $S(k)$ from the GFMC results confirms that these are excellent pseudopotentials.

It is not possible to use the PPA method of Pinski-Campbell in the crystal phase since the HNC method employed to perform the iterations can only be applied in the liquid phase. We chose instead a wave function with the McMillan form^{3(a)} of the pseudopotential plus a localized (one-body) Gaussian

$$\psi^{(0)}(R) = \exp\left[-\frac{1}{2} \sum_{i < j} u(r_{ij})\right] \prod_m \phi(r_m - S_m), \quad (3.3)$$

S_m are the lattice sites. Variational calculations were performed with this wave function to minimize the energy and the resulting parameters were then used in the GFMC calculations which converged satisfactorily.

As mentioned above, we used Rayleigh-Schrödinger theory (RS) to predict the energy of a many-body ⁴He system using various two-body potentials. To lowest order in ΔV , the eigenvalue per particle of He is given by

$$E_0^V = E_0^{LJ} + \frac{1}{2} \rho \int d^3r \Delta V g_{LJ}(r) d^3r, \quad (3.4)$$

$$\Delta V = \sum_{i < j} (V_{ij} - V_{ij}^{LJ}),$$

where V_{ij}^{LJ} is the Lennard-Jones potential at r_{ij} and V_{ij} is some other potential at the same point. $g_{LJ}(r)$ is the radial distribution function obtained from the GFMC simulation of LJ ⁴He and E_0^{LJ}/N is the energy per particle derived from the same calculations. The energy from this perturbation theory is an upper bound to the exact eigenvalue. In Table I, where we compare variational, perturbation theory, and GFMC results for E_0 with various potentials, we see that the

TABLE I. Summary of energies (E_2) in liquid ⁴He from variational, perturbation theory, and GFMC calculations. All energies are given in kelvin per particle.

Potential	$\rho\sigma^3$	Variational	$\rho\sigma^3$	Perturbation	$\rho\sigma^3$	GFMC
Lennard-Jones	0.365	-5.68	0.365	-6.85
Beck ^a	0.306	-5.62	0.365	-6.57
FDD-1 ^b	0.325	-7.10	0.365	-8.39
MDD-2 ^b	0.300	-5.67	0.365	-6.48
ESMMSV	0.365	...	0.365	-6.32	0.365	-6.49
MS12G6	0.365	...	0.365	-7.68	0.365	-7.84
HFDHF2	0.365	-5.87	0.365	-6.98	0.365	-7.12

^aR. D. Murphy, Phys. Rev. A 5, 331 (1972).

^bR. D. Murphy and R. O. Watts, J. Low Temp. Phys. 2, 507 (1970).

perturbation theory result is consistently within 0.12 K of the GFMC result. Therefore we are confident that our perturbation results are reliable indicators of the behavior for potentials in which we did not pursue GFMC calculations.

We estimated the contribution of three-body terms to the potential by calculating the perturbation of the energy arising from the Axilrod-Teller triple-dipole potential,¹⁹

$$V_3(r_{12}, r_{13}, r_{23}) = \frac{0.324 \left(1 + 3 \prod_{i=1}^3 \cos \theta_i \right)}{r_{12}^3 r_{13}^3 r_{23}^3} \quad (3.5)$$

Barker argues that this form of the three-body potential is the major contributor to the energy. In Appendix A of WCK, we described in detail how we estimated this perturbative correction. We note here that the values of the three-body correction given in WCK for liquid and solid LJ ⁴He are in error by a few percent. We shall correct these values in the following section.

IV. RESULTS

As mentioned above, we used first-order perturbations from our exact LJ results to suggest which potentials to use in GFMC calculations. In Table I we have summarized the results from our perturbation calculations, various variational calculations, and our GFMC calculations at the density at which the energy is smallest. From the perturbation data, it is clear that the HFDHE2 is the most promising potential to use in many-body theories. Though the ESMMSV

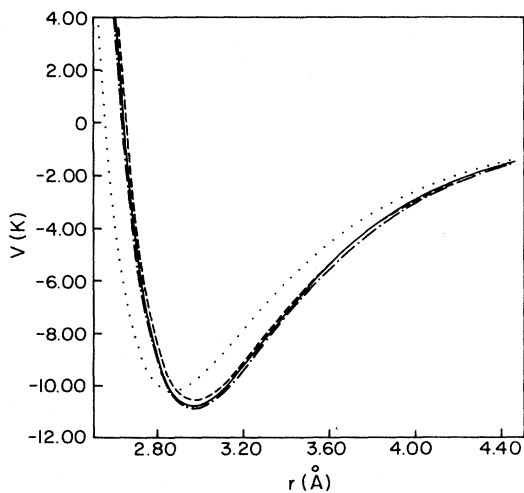


FIG. 1. Comparison of the potential energy as a function of distance for several two-body ⁴He potentials. The potentials are identified as follows: (. . .) Lennard-Jones, (—) HFDHE2, (- · -) MS12G6, and (- - -) ESMMSV.

TABLE II. Energy and length parameters for several potentials.

	ϵ (K)	r_m (Å)
Lennard-Jones	10.22	2.869
ESMMSV	10.57	2.97
MS12G6	10.9	2.967
HFDHE2	10.8	2.9673

and the MS12G6 potentials gave energies which were too high and too low, respectively, we decided to use them in GFMC simulations since they did reasonably well in reproducing experimental two-body data in the calculations of Aziz *et al.*¹² A glance at Fig. 1 or Table II reveals that the ordering of the simple perturbation energies of the three potentials follows that of their well depth. The position of the minimum is very similar for the potentials and within the experimental uncertainty as derived from molecular measurements. One might expect that the many-body energies would be much closer than they are, especially for the MS12G6 and HFDHE2 potentials. The behavior predicted by perturbation theory is confirmed by the GFMC calculations. The only acceptable potential of the three is HFDHE2 and it reproduces the experimental equation of state very well. The energy of the many-body system appears to be very sensitive to minor changes in the shape of the potential and this is reflected in the GFMC results. The real puzzle in this investigation of various ⁴He potentials is the LJ potential. Its energy is closer to the experimental equation of state than either the MS12G6 or ESMMSV potential; however, neither the position of the well nor the well depth are in the range which gives agreement with experiment. We conjecture that it is largely fortuitous that the LJ potential provides a reasonable description of the properties of liquid ⁴He. Similar behavior occurs with the LJ potential for argon.^{1(a)} In that case, the LJ potential gives a good agreement with experimental data on the liquid state if many-body interactions are neglected. However, the well depth of the LJ potential is known to be in error by 20% and the coefficient of R^{-6} at large distances is in error by a factor of 2.

A. Equation of state: Liquid phase

After the excellent showing of the HFDHE2 potential at the experimental equilibrium density, we pursued GFMC simulations at several other densities. The energies are compared with those of other potentials and experiment²⁰ in Fig. 2. Table III contains a

TABLE III. Energies in the liquid phase from the GFMC calculations with the HFDHE2 potential, the Lennard-Jones potential, and experiment. The first column gives the density in reduced units; E_2 is the eigenvalue from the GFMC calculations; $\langle V_3 \rangle$ is the perturbation estimate of V_3 , $E = E_2 + \langle V_3 \rangle$; and E_{expt} is the experimental value of the energy from Ref. 20. All energies are in kelvin per particle.

$\rho\sigma^3$	E_2	HFDHE2 $\langle V_3 \rangle$	E	E_2	Lennard-Jones $\langle V_3 \rangle$	E	E_{expt}
0.328	-7.034 ± 0.037	0.113 ± 0.002	-6.921 ± 0.037	-6.662 ± 0.035	0.114 ± 0.002	-6.627 ± 0.035	...
0.365	-7.120 ± 0.024	0.152 ± 0.003	-6.968 ± 0.024	-6.848 ± 0.018	0.149 ± 0.003	-6.699 ± 0.018	-7.14
0.401	-6.894 ± 0.048	0.190 ± 0.002	-6.704 ± 0.048	-6.743 ± 0.033	0.195 ± 0.001	-6.548 ± 0.033	-7.00
0.438	-6.564 ± 0.058	0.237 ± 0.003	-6.327 ± 0.058	-6.386 ± 0.072	0.244 ± 0.002	-6.142 ± 0.072	-6.53
0.490	-5.175 ± 0.101	-5.362 ± 0.079	0.325 ± 0.004	-5.037 ± 0.079	...

comparison of the GFMC energies calculated with the LJ and the HFDHE2 potentials. We have reported the densities in units of σ^{-3} to make comparison with our earlier LJ results easier. By multiplying densities in units of atoms/ σ^3 by 0.059 89, units of atoms/ \AA^3 are obtained. Except for the value at $\rho\sigma^3 = 0.4013$, the HFDHE2 energies are within their standard deviations of the experimental energies. Thus the shape of the equation of state is reproduced well by the HFDHE2 potential.

In columns 3 and 6 of Table III we give our estimates of the Axilrod-Teller three-body corrections to

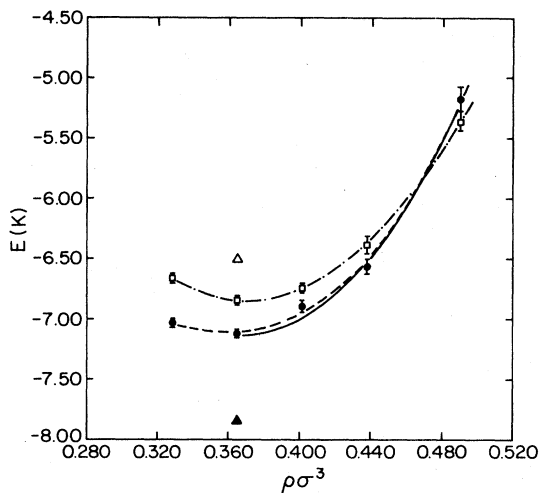


FIG. 2. Equation of state for the liquid phase of ^4He . The solid line represents the experimental equation of state of Ref. 20. The solid circles are the GFMC energies with the HFDHE2 potential; the dashed line is a fit to the calculated energies. The boxes are GFMC energies with the Lennard-Jones potential and the dashed-dot line is a fit to the latter energies. The triangle is the GFMC energy calculated with the ESMMSV potential and the solid triangle is the GFMC energy calculated with the MS12G6 potential.

the energy of the HFDHE2 and LJ systems, respectively. As noted above, the values of $\langle V_3 \rangle$ for LJ are corrected slightly from those given in WCKK. The values of the three-body energies in the two systems are identical within their errors and are in agreement with the calculations of Murphy and Barker.^{1(b)} The sign of $\langle V_3 \rangle$ is positive and increases the energies. Thus the energy, E , of the HFDHE2 system is no longer in agreement with experiment but differs by about 0.2 K. Note, however, that the calculation of $\langle V_3 \rangle$ is in effect an estimate of the RS perturbative effect of V_3 and hence yields an upper bound to the energy.

The sensitivity of the many-body energy to small changes in the two-body potential is an interesting phenomenon. We investigated this phenomenon further by observing how the energy changed when the HFDHE2 potential parameters were varied within reasonable limits. Table IV summarizes the results

TABLE IV. Energies of ^4He system when the HFDHE2 potential parameters are varied. The first column gives the density in reduced units; r_m and ϵ are the length and energy parameters; the fourth column is E_2 as predicted by perturbation theory; and the last column gives the GFMC energy. All energies are in kelvin per particle.

$\rho\sigma^3$	r_m (\AA)	ϵ (K)	Perturbation theory	GFMC
0.3648	2.9673	11.0	-7.52	-7.548 ± 0.029
0.4378	2.9673	11.0	-7.06	-7.003 ± 0.016
0.491 ^a	2.9673	11.0	-6.20	-6.237 ± 0.038
0.3283	2.9648	10.8	-7.01	-6.952 ± 0.026
0.3648	2.9648	10.8	-7.09	-7.075 ± 0.040
0.4013	2.9648	10.8	-6.87	-6.736 ± 0.026
0.4378	2.9648	10.8	-6.54	-6.404 ± 0.026

^afcc crystal.

of changing the potential parameters. First we decreased the value of ϵ from 10.8 to 11.0 K, and performed GFMC simulations at two densities in the liquid. The energies decreased by about 0.45 K from the values for the unperturbed HFDHE2 potential. Figure 3 shows the changed energies compared with the unperturbed HFDHE2 energies. It appears that increasing the value of ϵ has shifted the equation of state to lower energies but has not affected its shape. We performed additional RS perturbation calculations starting from our $g(r)$ obtained using HFDHE2 rather than those obtained from LJ. These gave very good predictions of the change in energy. RS theory, being first order in ΔV , is equivalent to the Hellmann-Feynman theorem which here reduces to $\partial E/\partial \epsilon = \langle V \rangle/\epsilon_0$.

The next variation of a parameter we tried was to change r_m from 2.9673 to 2.9648 Å. As can be seen in Fig. 3 and Table IV, this very small change in the position of the minimum significantly changed the equation of state. The equilibrium density has shifted to a lower density and the curvature of the equation of state became steeper. The results from a perturbation calculation predict the trends observed in the GFMC simulation. The primary contribution to the integral in Eq. (3.4) occurs at small values of r , where $g(r)$ is least accurate. These uncertainties are reflected in the perturbation energies as an error estimated to be 0.2 K.

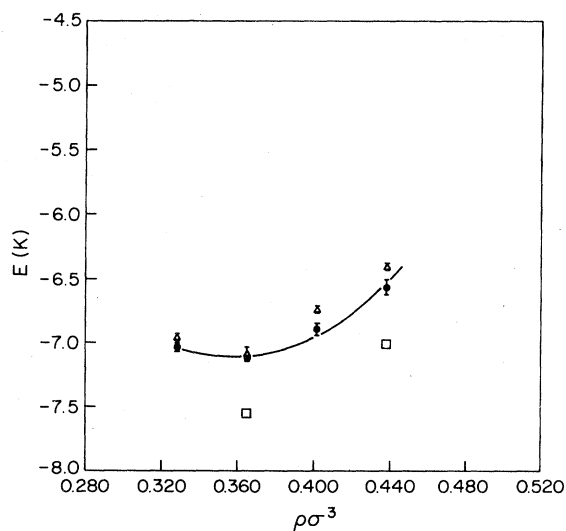


FIG. 3. Effect of changing the HFDHE2 potential parameters on the equation of state. The solid circles are the GFMC energies with the original HFDHE2 potential and the solid line is a fit to the calculated energies. The boxes represent GFMC energies with a modified HFDHE2 potential where $\epsilon = 11.0$ K and $r_m = 2.9673$ Å. The triangles are GFMC energies for a modified HFDHE2 potential where $\epsilon = 10.8$ K and $r_m = 2.9648$ Å.

The results of changing the HFDHE2 parameters indicate that any improvements in the many-body energy will require delicate tuning of the parameters. Small changes in the value of r_m within the estimated standard error range lead to relatively large changes in energy. Such tuning can be done rather easily and reliably by using Eq. (3.4) and the radial distributions in the Appendix.

B. Radial distribution function and structure function

Other properties of HFDHE2 liquid ^4He were investigated as well. In Fig. 4, we show the radial distribution function from the GFMC calculation (solid line) at a density of $\rho\sigma^3 = 0.3648$ in comparison with an experimental $g(r)$ shown by circles derived from the measurements of Sears and co-workers.²¹ The experimental $g(r)$ was obtained by Fourier transforming the $S(k)$ measured at saturated vapor pressure at 1.0 K. Agreement between the theoretical and the experimental pair correlation function is excellent and demonstrates that the HFDHE2 potential gives a good representation of pair correlations in liquid helium. The width and the height of the first peak in $g(r)$ are especially well reproduced in the GFMC calculation. The $g(r)$ derived from GFMC calculations with the HFDHE2 potential has a sharper first peak by about 2% than the $g(r)$ from LJ GFMC calculations.^{10(b)}

Figure 5 contains a comparison of the GFMC with

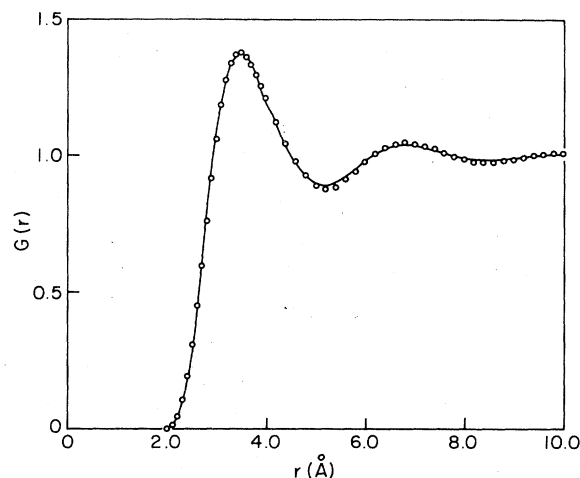


FIG. 4. Comparison of the calculated and experimental radial distribution function. The solid line gives $g(r)$ at $\rho\sigma^3 = 0.3648$ derived from the GFMC calculations with the HFDHE2 potential. The circles are experimental points given in Ref. 21 derived from neutron diffraction measurements at saturated vapor pressure at 1.0 K.

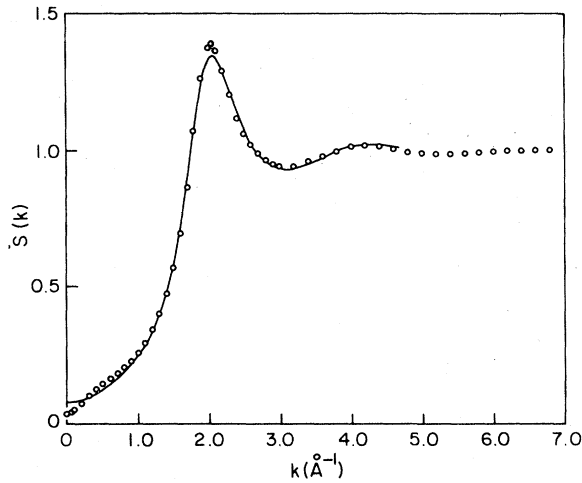


FIG. 5. Comparison of the calculated and experimental structure function. The solid line is $S(k)$ at $\rho\sigma^3 = 0.3648$ which is the Fourier transform of the calculated $g(r)$ in Fig. 4. The circles are the smoothed $S(k)$ measured by neutron diffraction at saturated vapor pressure at 1.0 K, described in Ref. 21.

the HFDHE2 potential and an experimental structure function, $S(k)$. The GPMC $S(k)$ is at a density of $\rho\sigma^3 = 0.3648$ and is the Fourier transform of $g(r)$ shown in Fig. 4. The experimental $S(k)$ is a smoothed version of the structure function measured by Sears and co-workers by neutron diffraction at 1.0 K at saturated vapor pressure. $S(k)$ derived from the HFDHE2 is in better agreement with the neutron-diffraction experiments than the LJ potential though there are still discrepancies in the vicinity of the first maximum. $S(k)$ derived from the LJ GPMC calculations is about 3% lower at the first peak than $S(k)$ from the present GPMC calculations. The discrepancy between experiment and the present GPMC result is not dramatic, however, since the $S(k)$ values are within each other's error. This is clearly shown in Fig. 6. Figure 6 displays the value of $S(k)$ at its maximum as a function of temperature. The GPMC value (■) is shown at 0 K. The x-ray diffraction results of Robkoff, Ewen, and Hallock²² are plotted as (▲) and the neutron diffraction results of Sears and co-workers are plotted as (■). Sears *et al.* estimated that their statistical precision is 0.8% and the residual systematic error is less than 1%. These errors are shown separately on two of the data points to indicate how the experimental errors compare with the GPMC errors. In a paper which discusses the static structure function measured in the neutron diffraction experiments, Svensson *et al.*²³ argue that $S(k)$ changes very little below 1.0 K. They compare the results of a recent calculation²⁴ of the temperature variation of $S(k)$ due to the thermal

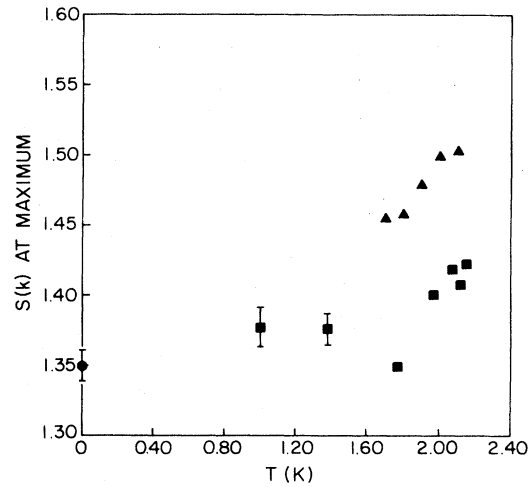


FIG. 6. Maximum value of $S(k)$ as a function of temperature at saturated vapor pressure. The GPMC value is represented by a circle at $T = 0$ and $\rho\sigma^3 = 0.3648$. The triangles (▲) are derived from x-ray diffraction experiments of Ref. 22. The squares are values of maximum $S(k)$ measured in the neutron diffraction experiments of Ref. 21. The error bars represent, respectively, a residual systematic error of $\sim 1.0\%$ and the statistical precision of 0.8% in the experimental measurement.

excitation of rotons out of a Jastrow ground state with the experimental temperature variation. The theoretical change in $S(k)$ between $T = 0$ and $T = 2.1$ K is in reasonable agreement with the experimental change between $T = 1.00$ and $T = 2.12$ K. Thus Svensson *et al.* conclude that their $S(k)$ at 1.0 K is essentially the same as $S(k)$ at $T = 0$ and can be compared with theoretical estimates at $T = 0$. $S(k)$ derived from the GPMC HFDHE2 calculations is sharper than $S(k)$ derived from calculations which used the LJ potential and is therefore in better agreement with recent experimental measurements.

C. Momentum distribution

We have determined the value of n_0 , the fraction of particles in the zero-momentum state, at $\rho\sigma^3 = 0.3648$ to be 0.090 ± 0.003 . This can be compared with the previous theoretical value of 0.113 ± 0.002 obtained from the LJ GPMC calculations. The difference between the values of n_0 is significant and is larger than would have been anticipated from earlier simulation studies of hard-sphere systems.^{11(b)} However, Lam and Chang²⁵ report similar differences in the condensate fraction when the potential is changed. The most recent experimental determinations of n_0 have used the theory proposed by Cum-

mings, Hyland, and Rowlands²⁶ to extract n_0 from $g(r)$. Cummings *et al.* suggest that the condensate fraction is related to the behavior of $g(r)$ at large r upon crossing the λ transition. That is,

$$n_0 = 1 - \left(\frac{g(r, T^-) - 1}{g(r, T^+) - 1} \right)^{1/2}, \quad (4.1)$$

where $g(r, T^\pm)$ is the pair correlation function just above (+) and below (-) the λ transition. The expression is expected to be valid for $r > 4.5 \text{ \AA}$ where the reduced one-particle density matrix approaches n_0 . Robkoff, Ewen, and Hallock²² have analyzed their x-ray data using Eq. (4.1) and report values of $9 \pm 3\%$ at $T^- = 1.67 \text{ K}$ and $T^+ = 2.20 \text{ K}$ at saturated vapor pressure and $8 \pm 3\%$ when $T^- = 1.7 \text{ K}$ at $\rho = 0.378 \sigma^{-3}$ for n_0 . Sears and Svensson²⁷ performed a similar analysis on their neutron diffraction data and found n_0 over a range of temperatures. Their results for n_0 are well represented by

$$n_0(T) = n_0(0) [1 - (T/T_\lambda)^\alpha], \quad (4.2)$$

with $n_0(0) = 13.3 \pm 1.2\%$ and $\alpha = 6.2 \pm 1.6$. The GFMC and experimental values for n_0 are in satisfactory agreement; however, the validity of Eq. (4.1) has yet to be rigorously established so these experimental values should still be considered tentative.

In Fig. 7, we present the momentum distribution from our GFMC calculations plotted as $kn(k)$. The solid line is the GFMC results with the HFDHE2 potential and the dashed line represents the experimen-

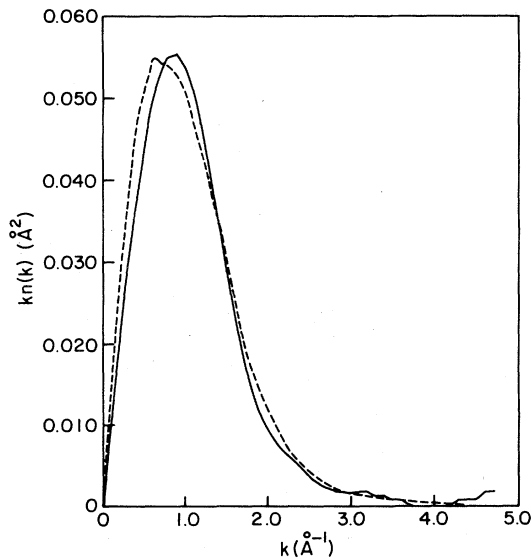


FIG. 7. Comparison of the calculated and experimental momentum distribution plotted as $kn(k)$. The solid line is the GFMC result. The dashed line is the experimental results of Ref. 28.

tal values of Woods and Sears²⁸ obtained from neutron scattering data. The structure at large k of the GFMC results are within our errors which are approximately 10%. The agreement between the theoretical and experimental momentum distributions is very good; any differences are within the errors of the two sets of results. Overall the HFDHE2 potential is seen to give a very good account of the interactions in liquid ^4He .

D. Equation of state: crystal phase

We have used the HFDHE2 potential to calculate the energy of the fcc crystal in the density range $\rho\sigma^3 = 0.491$ to 0.589 . We limited our GFMC simulations to the fcc phase because our earlier results^{10(a)} with the LJ potential showed that we could not distinguish the hcp from the fcc phase and it is technically more convenient to calculate the latter. As mentioned above, we used a McMillan form of the pseudopotential plus a localized Gaussian in the importance function for the crystal phase. An importance function which localizes the particles on the lattice sites speeds the convergence of the GFMC iterations. The particular parameters in the importance function for each density were determined by a variational search for values that minimize the energy.

Our results for the crystal equation of state are shown in Fig. 8. The triangles are our GFMC results with the HFDHE2 potential and the solid line is a fit to them. The circles are the experimental measure-

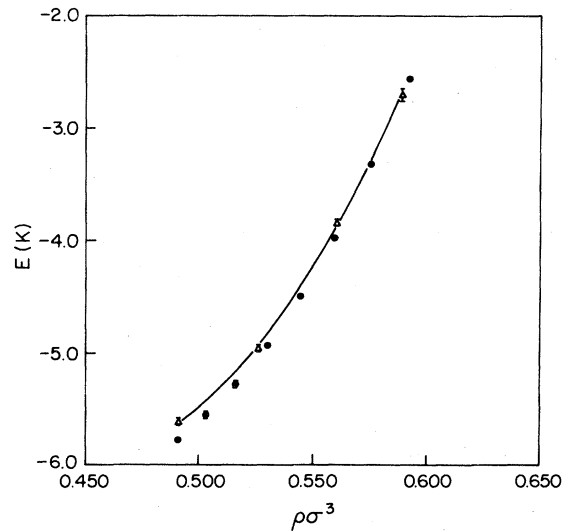


FIG. 8. Equation of state of solid ^4He . The triangles are the GFMC energies calculated with the HFDHE2 potential. The solid line is a fit to these energies. The solid circles are the energies of the hcp solid reported in Ref. 29 with two points showing the magnitude of the errors.

ments extrapolated to 0 K by Edwards and Pandorf.²⁹ The agreement between theory and experiment is good, especially at higher densities. By contrast GFMC calculation with the LJ potential gave an equation of state whose shape disagreed with experiment. In Table V the fcc crystal energies are given as a function of density and compared with experimental energies. Also included is our estimate of the Axilrod-Teller three-body perturbation energy at each energy. In all cases the perturbative correction is positive and when added to the GFMC E_2 , the resulting energy disagrees with experiment by about 0.5 K.

The discrepancy between the calculated total energy, $E = E_2 + \langle V_3 \rangle$, and experiment (cf. Tables III and V) is somewhat disturbing. While three-body interactions are anticipated to be small in comparison with two-body energies, their inclusion was expected to improve the agreement between theory and experiment. It occurred to us that perhaps a simple scaling of the potential might resolve the discrepancy. From Table III we have data from GFMC simulations with $\epsilon = 10.8$ and 11.0 K at ρ_0 and $1.2\rho_0$. Using linear interpolation, justified by the good results from RS perturbation theory, we determined a value of ϵ which should give E in agreement with experiment. This new value of ϵ is 10.88 K and we used it in a perturbation theory calculation of the many-body energies for both the liquid and the crystal phases. A summary of the perturbation results is given in Table VI. The scaling of ϵ works well in the liquid phase with the values of E within their errors of experiment. This is shown in Fig. 9. The results are not as promising in the crystal phase. The decrease in E_2 due to the larger value of ϵ is not sufficient to compensate for the three-body energy correction. We can

TABLE V. Energies in the fcc crystal phase. Column one gives the density in units of σ^3 . The second column contains the GFMC HFDHE2 energy while the next column is our estimate of the Axilrod-Teller, three-body perturbation correction to the energy. Column four is the sum of E_2 and $\langle V_3 \rangle$ and E_{expt} is the experimental value for the energy. All energy values quoted in kelvin per particle.

$\rho\sigma^3$	E_2	$\langle V_3 \rangle$	E	E_{expt}^a
0.491	-5.61 ± 0.03	0.32	-5.29 ± 0.03	-5.78 ± 0.05
0.526	-4.94 ± 0.03	0.39	-4.55 ± 0.03	-5.03 ± 0.05
0.56	-3.87 ± 0.03	0.47	-3.40 ± 0.03	-3.94 ± 0.05
0.589	-2.68 ± 0.06	0.65	-2.03 ± 0.06	-2.70 ± 0.05

^aD. O. Edwards and R. C. Pandorf, Phys. Rev. **140**, A816 (1965). Values are interpolated between their energy measurements for hcp ^4He at 0 K.

TABLE VI. Summary of perturbation energies for the HFDHE2 potential with $\epsilon/k = 10.88$ K. Column one contains the density in reduced units. In column two are the perturbative estimate estimates of E_2 . Column three contains the perturbative $E_2 + \langle V_3 \rangle$ and column four gives experimental energies. All energies are quoted in kelvin per particle.

$\rho\sigma^3$	Perturbation theory	Perturbation energy $+ \langle V_3 \rangle$	E_{expt}
Liquid			
0.3283	-7.17	-7.06	-7.01 ^a
0.3648	-7.28	-7.13	-7.14 ^a
0.4013	-7.07	-6.88	-7.00 ^a
0.4378	-6.77	-6.53	-6.53 ^a
Crystal			
0.491	-5.84	-5.52	-5.78 ^b
0.526	-5.19	-4.80	-5.03 ^b
0.56	-4.13	-3.67	-3.94 ^b
0.589	-2.95	-2.30	-2.70 ^b

^aReference 20.

^bReference 28.

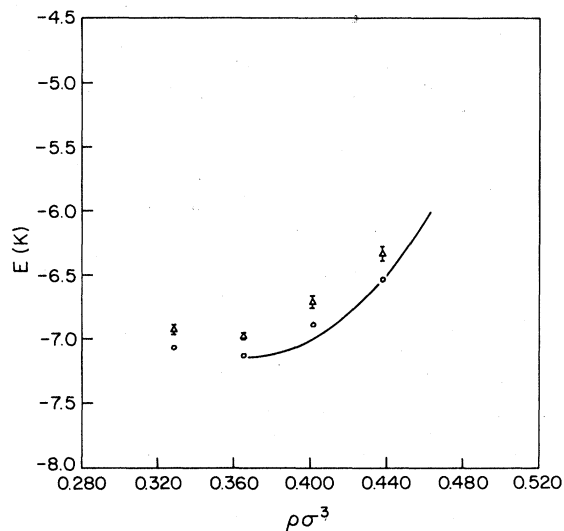


FIG. 9. Effect of deepening the HFDHE2 potential on the equation of state of the liquid. The solid line is the experimental equation of state as described in Ref. 20. The circles are the perturbation estimate of E_2 with the HFDHE2 potential when $\epsilon = 10.88$ K plus $\langle V_3 \rangle$. The triangles are GFMC energies with the original HFDHE2 potential plus $\langle V_3 \rangle$.

correct the energies of either the liquid or the crystal phase by our simple scaling of the potential, but not both phases. It is clear that a more sophisticated treatment of the potential is required in order that the many-body energy calculated with two-body and three-body potentials agree with experiment at all densities in both the liquid and crystal phases.

E. Melting-freezing transition

We fit our equation of state in the liquid and crystal phases to functions of the form

$$E = E_0 + B \left(\frac{\rho - \rho_0}{\rho_0} \right)^2 + C \left(\frac{\rho - \rho_0}{\rho_0} \right)^3. \quad (4.3)$$

A similar function has been used to fit experimental equations of state²⁰ and we used this form to analyze our LJ GFMC results,¹⁰ as well. The experimental equation of state reported by Roach, Ketterson, and Woo^{20(a)} used Eq. (4.3) to fit values of $E(\rho)$ obtained from integrating the pressure as a function of density. Aziz and Pathria^{20(b)} obtained a power series in $(\rho - \rho_0)/\rho_0$ for the equation of state from a series expansion of the density dependence of the speed of sound. In the density range we investigated, the two experimental fits are the same within the accuracy plotted and are shown by the solid line in Fig. 2. For the liquid phase without three-body corrections the values of the parameters in Eq. (4.3) are

$$E_0 = -7.110 \pm 0.023, \quad B = 10.08 \pm 3.2, \\ \rho_0 = 0.3600 \pm 0.0049, \quad C = 12.59 \pm 8.5. \quad (4.4)$$

The quoted errors were determined from the errors of the GFMC energies and are correlated. These correlations were taken into account in calculating the errors of functions depending on E_0 , B , C , and ρ_0 . The analytical fit to the liquid equation of state is shown as a dashed line in Fig. 2.

We determined an analogous fit to our crystal data which yields

$$E_0 = -5.899 \pm 0.121, \quad B = 31.95 \pm 5.26, \\ \rho_0 = 0.4486 \pm 0.0097, \quad C = 3.395 \pm 80.0. \quad (4.5)$$

This representation of the crystal equation of state is not the best least-squares fit because of the limited number of densities we studied in the GFMC simulation. It is, however, a very reasonable fit as can be seen in Fig. 8. The two analytical equations of state were then used to determine the melting and freezing densities via a Maxwell (double-tangent) construction. In Table VII, the melting and freezing densities are given for ⁴He calculated using HFDHE2, LJ, and obtained from experiment. The HFDHE2 liquid freezes at a density of $0.438/\sigma^3$ which is only 2% above the freezing density observed in experiment. The solid melts at a density $0.491/\sigma^3$, which is 5% above that of experiment. This discrepancy is a reflection of the difference in behavior of the equation of state of the HFDHE2 simulation and experiment at lower crystal densities. The pressure at the double-tangent densities is 26.7 atm, which is within one standard error of the experimental pressure. The volume variation, $2.47 \text{ cm}^3/\text{mol}$, is significantly larger than that observed in experiment.

F. Isothermal compressibility

The last property of HFDHE2 helium we will present are the isothermal compressibilities of the liquid and crystal phase. The isothermal compressibility is defined as

$$\kappa = \frac{1}{\rho} \left(\frac{\partial \rho}{\partial P} \right)_T, \quad (4.6)$$

where $P(\rho) = \rho^2 \partial E / \partial \rho$ is the pressure. Equation

TABLE VII. Melting-freezing transition. A comparison of the GFMC calculations with the HFDHE2 potential, with the Lennard-Jones potential and with experiment. The first column identifies the system, the second and third columns give the freezing and melting densities in reduced units, column four is the pressure at the transition and column five is the volume difference between the two phases at the transition.

Potential	$\rho_l \sigma^3$	$\rho_s \sigma^3$	p (atm)	ΔV (cm^3/mol)
HFDHE2	0.438 ± 0.011	0.491 ± 0.010	26.73	2.47
LJ	0.475 ± 0.011	0.515 ± 0.009	42.85 ± 8.64	1.63
Experiment	0.430	0.468	25.0	1.9

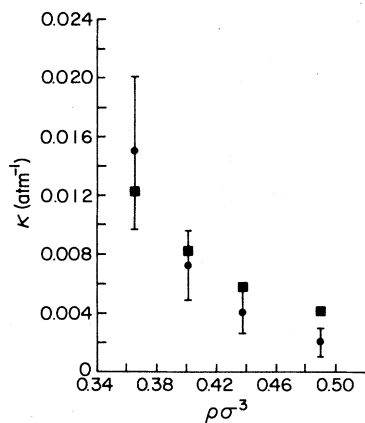


FIG. 10. Isothermal compressibility of the liquid phase plotted vs density. The solid circles with error bars are the values from the GPMC calculation with the HFDHE2 potential. The solid squares are derived from the experimental equation of state of Ref. 20(a).

(4.3) then gives the expression

$$\kappa = \frac{1}{2} \left(\frac{\rho_0}{\rho^2} \right) \left\{ B \left[3 \left(\frac{\rho}{\rho_0} \right) - 2 \right] + 3C \left[2 \left(\frac{\rho}{\rho_0} \right)^2 - 3 \left(\frac{\rho}{\rho_0} \right) + 1 \right] \right\}^{-1} \quad (4.7)$$

The behavior of κ as a function of density is a severe test of a theoretical equation of state. Figure 10 shows the isothermal compressibility for the liquid phase from the GPMC calculations compared with that derived from the experimental equation of state of Roach, Ketterson, and Woo.^{20(a)} The GPMC result is within two standard errors of the experimental

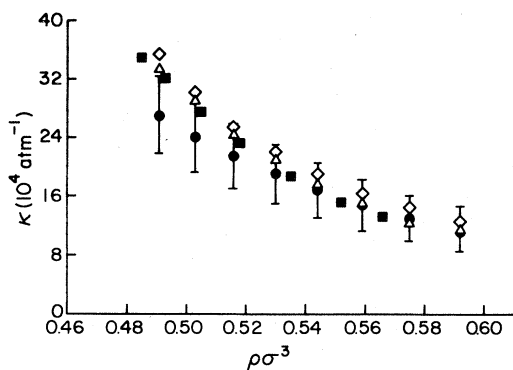


FIG. 11. Isothermal compressibility of the crystal phase plotted vs density. The solid circles with error bars are the values from the GPMC calculation with the HFDHE2 potential. The remaining symbols represent experimental measurements; (■) Ref. 30(b), (Δ) Ref. 29, and (\diamond) Ref. 30(a).

value at all densities. The density dependence of the theoretical and experimental values is somewhat different, reflecting the slight difference in shape of the two equations of state. A comparison of κ calculated from the GPMC results for the crystal phase with several experimental determinations^{29,30} as a function of density is given in Fig. 11. At low densities, the calculated κ is lower than experiment but within two standard errors. At higher densities the calculated κ agrees with experiment which would be expected from the equation of state.

V. CONCLUSIONS

We have investigated the effect of several two-body potentials on the equilibrium energy of liquid ^4He using the Green's-function Monte Carlo method. One potential, the HFDHE2 potential, proposed by Aziz *et al.*, gave excellent agreement with experiment. The HFDHE2 potential was then used in a GPMC calculation to determine the equation of state of liquid and fcc crystal ^4He . Within the statistical sampling errors, the calculated liquid equation of state agrees with experiment. The lowest crystal energies are somewhat higher than experiment at the lowest densities but agree with experiment above $\rho\sigma^3 = 0.525$. Overall the agreement between the GPMC calculations and experiment is very good. However, if an estimate of the Axilrod-Teller three-body energy is added as a correction to the GPMC energy, the calculated equation of state is shifted to higher energies. An attempt was made to derive a better two-body potential by slightly deepening the HFDHE2 potential. Perturbation-theory calculations, indicate that this does not work in both the liquid and crystal phases. Further investigation of the role of two- and three-body interactions in ^4He is needed.

The radial distribution function derived from the GPMC calculation at the equilibrium density compares well with $g(r)$ derived from neutron diffraction experiments.²¹ However, the experimental structure function from neutron diffraction exhibits a slightly sharper first peak than the calculated $S(k)$. Analysis of the relevant errors suggests that experiment and theory are within each others errors. $S(k)$ from x-ray diffraction experiments²² is significantly higher valued than the neutron diffraction results at similar temperatures. If the resolution of the experimental differences are resolved in favor of a sharper first peak of $S(k)$, an obvious discrepancy with theory will result. In that case, it would be interesting to see whether the RS perturbation theory we have used for estimating three-body potential corrections is correct or whether a significant rearrangement of the three-body correlations occurs. One might then find a sharper structure and a lower energy than that given by the perturbation estimate. It is not clear whether

three-body forces are well enough understood in ${}^4\text{He}$ to make straightforward inclusion in the GFMC calculation worthwhile.

Other properties of liquid ${}^4\text{He}$ derived from the GFMC simulation such as the momentum-condensate fraction and the momentum distribution compare well with experimental determinations. In the crystal phase, the isothermal compressibility is close to experiment at higher densities as would be expected from the equation of state. Overall, the HFDHE2 potential gives a very satisfactory description of the properties of liquid and solid ${}^4\text{He}$. Minor modification of the potential parameters may improve agreement between experiment and the calculated solid equation of state. Until such an improvement is attained, we recommend that theorists adopt the HFDHE2 potential for future calculations of ${}^4\text{He}$.

ACKNOWLEDGMENTS

We are indebted to many colleagues for enlightening comments and conversations; these include L. W.

Bruch, R. A. Aziz, K. Schmidt, and S. Borowitz. We are grateful to L. Whitney and C. E. Campbell for supplying us the pseudopotentials we needed for liquid ${}^4\text{He}$ calculations with the HFDHE2 potentials. We also thank F. T. Pinsky for supplying us with a copy of the PPA code used to generate the pseudopotentials. R. B. Hallock and V. F. Sears kindly shared experimental data prior to publication. We thank P. Axelrod and V. Makarov for skillful programming assistance. This work was supported in part by the U.S. DOE Contract No. DE AC02-76ER03077 and in part by the National Science Foundation under Grant No. DMR-77-18329.

APPENDIX: TABULATED RADIAL DISTRIBUTION FUNCTIONS

In this Appendix we present tables of $g(r)$ in the liquid and fcc crystal phases at several densities. R is in units of \AA and denotes the midpoint of the interval for which $g(r)$ is given. The densities ρ are in units of σ^{-3} .

TABLE VIII. $g(r)$ in the liquid and fcc crystal phases.

$R/\rho =$	Liquid phase			
	0.3284	0.3648	0.4013	0.4378
1.687	0.0000	0.0000	0.0000	0.0000
1.789	0.0000	0.0000	0.0000	0.0009
1.891	0.0004	0.0000	0.0001	0.0021
1.994	0.0024	0.0037	0.0015	0.0030
2.096	0.0184	0.0133	0.0053	0.0087
2.198	0.0327	0.0361	0.0373	0.0413
2.300	0.0941	0.0952	0.1100	0.0902
2.403	0.1387	0.1710	0.2114	0.1696
2.505	0.2897	0.2809	0.3272	0.3743
2.607	0.3887	0.4663	0.4949	0.5602
2.709	0.5188	0.6316	0.6686	0.6966
2.812	0.7395	0.8376	0.8890	0.8916
2.914	0.9202	0.9828	1.0210	1.0751
3.016	1.0475	1.1233	1.2003	1.3106
3.118	1.1430	1.2163	1.2933	1.3602
3.221	1.1983	1.3065	1.3895	1.4280
3.323	1.2816	1.3456	1.3770	1.5401
3.425	1.3251	1.3739	1.4132	1.4932
3.527	1.3042	1.3812	1.4401	1.5099
3.630	1.3194	1.3601	1.3969	1.4108
3.732	1.2748	1.3328	1.3557	1.3344
3.834	1.2832	1.2787	1.2838	1.2942
3.936	1.2148	1.2072	1.2416	1.2152
4.038	1.2428	1.1779	1.1896	1.1247
4.141	1.1458	1.1434	1.1238	1.0961
4.243	1.1299	1.0914	1.0512	1.0391
4.345	1.1120	1.0542	1.0225	0.9860
4.447	1.0863	1.0028	0.9749	0.9387
4.550	1.0106	0.9848	0.9482	0.8985

TABLE VIII (Continued).

$R/\rho =$	Liquid phase			
	0.3284	0.3648	0.4013	0.4378
4.652	0.9839	0.9542	0.9162	0.8662
4.754	0.9609	0.9296	0.8911	0.8424
4.856	0.9418	0.9110	0.8729	0.8273
4.959	0.9266	0.8985	0.8617	0.8206
5.061	0.9155	0.8917	0.8572	0.8218
5.163	0.9082	0.8902	0.8587	0.8303
5.265	0.9046	0.8933	0.8656	0.8448
5.368	0.9042	0.9004	0.8771	0.8644
5.470	0.9068	0.9106	0.8921	0.8878
5.572	0.9120	0.9231	0.9099	0.9137
5.674	0.9192	0.9372	0.9293	0.9408
5.777	0.9281	0.9521	0.9495	0.9680
5.879	0.9382	0.9670	0.9696	0.9941
5.981	0.9490	0.9815	0.9889	1.0183
6.083	0.9602	0.9949	1.0067	1.0396
6.186	0.9714	1.0069	1.0224	1.0575
6.288	0.9822	1.0171	1.0356	1.0716
6.390	0.9924	1.0254	1.0462	1.0815
6.492	1.0017	1.0317	1.0539	1.0873
6.594	1.0100	1.0359	1.0587	1.0891
6.697	1.0171	1.0382	1.0608	1.0871
6.799	1.0229	1.0386	1.0603	1.0817
6.901	1.0274	1.0375	1.0575	1.0735
7.003	1.0306	1.0350	1.0527	1.0629
7.106	1.0326	1.0313	1.0463	1.0506
7.208	1.0333	1.0269	1.0387	1.0372
7.310	1.0330	1.0219	1.0303	1.0234
7.412	1.0317	1.0165	1.0216	1.0097
7.515	1.0296	1.0112	1.0128	0.9967
7.617	1.0268	1.0060	1.0044	0.9849
7.719	1.0235	1.0012	0.9966	0.9746
7.821	1.0198	0.9969	0.9896	0.9662
7.924	1.0159	0.9932	0.9838	0.9598
8.026	1.0120	0.9902	0.9791	0.9555
8.128	1.0080	0.9880	0.9756	0.9534
8.230	1.0043	0.9865	0.9734	0.9533
8.333	1.0008	0.9857	0.9725	0.9552
8.435	0.9976	0.9856	0.9727	0.9587
8.537	0.9948	0.9861	0.9740	0.9636
8.639	0.9924	0.9870	0.9761	0.9696
8.742	0.9905	0.9884	0.9790	0.9765
8.844	0.9891	0.9901	0.9825	0.9837
8.946	0.9882	0.9920	0.9863	0.9911
9.048	0.9877	0.9940	0.9903	0.9983
9.150	0.9876	0.9960	0.9943	1.0050
9.253	0.9879	0.9980	0.9982	1.0110
9.355	0.9885	0.9998	1.0018	1.0161
9.457	0.9895	1.0014	1.0050	1.0202
9.559	0.9906	1.0028	1.0077	1.0232
9.662	0.9919	1.0039	1.0099	1.0250
9.764	0.9933	1.0047	1.0115	1.0256
9.866	0.9948	1.0053	1.0125	1.0252
9.968	0.9963	1.0056	1.0130	1.0238
10.071	0.9978	1.0056	1.0128	1.0215
10.173	0.9992	1.0054	1.0122	1.0185

TABLE VIII (Continued).

$R/\rho =$	Crystal phase			
	0.4910	0.5260	0.5600	0.5890
1.687	0.0000	0.0000	0.0000	0.0000
1.789	0.0002	0.0002	0.0000	0.0001
1.891	0.0007	0.0005	0.0016	0.0009
1.994	0.0030	0.0053	0.0042	0.0041
2.096	0.0118	0.0184	0.0231	0.0232
2.198	0.0449	0.0481	0.0540	0.0606
2.300	0.1075	0.1046	0.1423	0.1395
2.403	0.2002	0.2316	0.2706	0.2689
2.505	0.3476	0.3802	0.4405	0.4795
2.607	0.5500	0.5726	0.6596	0.7112
2.709	0.7566	0.7942	0.8962	0.9630
2.812	0.9528	1.0420	1.1372	1.2297
2.914	1.1815	1.2685	1.3420	1.4533
3.016	1.3402	1.4228	1.5280	1.6167
3.118	1.4634	1.5653	1.6605	1.7187
3.221	1.5774	1.6619	1.7271	1.7657
3.323	1.5862	1.7032	1.7411	1.8047
3.425	1.6002	1.6657	1.7101	1.7338
3.527	1.5837	1.6343	1.6221	1.6451
3.630	1.5783	1.5742	1.5255	1.4820
3.732	1.4734	1.4676	1.3976	1.3461
3.834	1.3666	1.3489	1.2518	1.1931
3.936	1.2841	1.2165	1.1330	1.0450
4.038	1.1709	1.1024	1.0023	0.9323
4.141	1.0679	0.9851	0.9369	0.8023
4.243	0.9770	0.8870	0.8421	0.7094
4.345	0.8891	0.7948	0.7634	0.6514
4.447	0.8193	0.7429	0.7037	0.6126
4.550	0.7605	0.7052	0.6647	0.6030
4.652	0.7183	0.6609	0.6469	0.6078
4.754	0.6933	0.6465	0.6495	0.6352
4.856	0.6849	0.6590	0.6710	0.6720
4.959	0.6921	0.6703	0.7087	0.7140
5.061	0.7132	0.7087	0.7595	0.7791
5.163	0.7460	0.7578	0.8197	0.8473
5.265	0.7879	0.8079	0.8853	0.9308
5.368	0.8362	0.8792	0.9526	1.0023
5.470	0.8881	0.9292	1.0177	1.0707
5.572	0.9409	1.0085	1.0773	1.1407
5.674	0.9920	1.0508	1.1286	1.2020
5.777	1.0393	1.1122	1.1695	1.2420
5.879	1.0808	1.1603	1.1983	1.2540
5.981	1.1151	1.1911	1.2145	1.2484
6.083	1.1412	1.2057	1.2179	1.2353
6.186	1.1585	1.2211	1.2093	1.1947
6.288	1.1670	1.1983	1.1899	1.1641
6.390	1.1669	1.1860	1.1614	1.1267
6.492	1.1590	1.1568	1.1259	1.0852
6.594	1.1442	1.1230	1.0859	1.0422
6.697	1.1237	1.0908	1.0438	1.0002
6.799	1.0991	1.0542	1.0019	0.9613
6.901	1.0717	1.0196	0.9626	0.9275
7.003	1.0430	0.9907	0.9277	0.9002
7.106	1.0145	0.9663	0.8989	0.8805
7.208	0.9875	0.9404	0.8774	0.8689
7.310	0.9632	0.9186	0.8638	0.8654

TABLE VIII (Continued).

$R/\rho =$	Crystal phase			
	0.4910	0.5260	0.5600	0.5890
7.412	0.9424	0.9025	0.8585	0.8696
7.515	0.9259	0.8924	0.8612	0.8807
7.617	0.9142	0.8884	0.8713	0.8976
7.719	0.9073	0.8901	0.8878	0.9190
7.821	0.9054	0.8972	0.9094	0.9433
7.924	0.9080	0.9089	0.9347	0.9690
8.026	0.9148	0.9243	0.9621	0.9945
8.128	0.9251	0.9422	0.9899	1.0186
8.230	0.9381	0.9618	1.0166	1.0399
8.333	0.9532	0.9819	1.0409	1.0575
8.435	0.9693	1.0014	1.0616	1.0707
8.537	0.9857	1.0195	1.0778	1.0791
8.639	1.0016	1.0353	1.0888	1.0824
8.742	1.0163	1.0483	1.0943	1.0810
8.844	1.0292	1.0580	1.0944	1.0752
8.946	1.0398	1.0641	1.0894	1.0657
9.048	1.0477	1.0666	1.0797	1.0531
9.150	1.0529	1.0657	1.0663	1.0385
9.253	1.0552	1.0616	1.0500	1.0227
9.355	1.0547	1.0547	1.0319	1.0068
9.457	1.0517	1.0455	1.0130	0.9915
9.559	1.0465	1.0348	0.9944	0.9778
9.662	1.0394	1.0230	0.9772	0.9662
9.764	1.0310	1.0109	0.9622	0.9573
9.866	1.0217	0.9991	0.9500	0.9513
9.968	1.0120	0.9881	0.9412	0.9484
10.071	1.0024	0.9785	0.9360	0.9486
10.173	0.9934	0.9706	0.9347	0.9516

¹(a) J. A. Barker, in *Rare Gas Solids*, edited by M. L. Klein and J. A. Verables (Academic, New York, 1976), Chap. IV. (b) R. D. Murphy and J. A. Barker, *Phys. Rev. A* **3**, 1037 (1971).

²J. de Boer and A. Michels, *Physica (Utrecht)* **5**, 945 (1938).

³(a) W. L. McMillan, *Phys. Rev. A* **138**, 442 (1965). (b) R. D. Murphy and R. O. Watts, *J. Low Temp. Phys.* **2**, 507 (1970).

⁴R. D. Murphy, *Phys. Rev. A* **5**, 331 (1972).

⁵K. Schmidt, M. H. Kalos, M. A. Lee, and G. V. Chester, *Phys. Rev. Lett.* **45**, 573 (1980); V. R. Pandharipande, *Phys. Rev. B* **18**, 218 (1978); C. C. Chang and C. E. Campbell, *ibid.* **15**, 4238 (1977).

⁶B. J. Jody, S. C. Saxena, V. P. S. Nain, and R. A. Aziz, *Chem. Phys.* **22**, 53 (1977).

⁷(a) J. M. Farrar and Y. T. Lee, *J. Chem. Phys.* **56**, 5801 (1972). (b) A. L. J. Burgmans, J. M. Farrar, and Y. T. Lee, *ibid.* **54**, 1345 (1976).

⁸B. Liu and A. D. McLean, unpublished calculation cited by Ref. 1(a).

⁹A. Michels, J. M. H. Levelt, and N. de Graaf, *Physica (Utrecht)* **24**, 659 (1958).

¹⁰(a) P. A. Whitlock, M. H. Kalos, G. V. Chester, and D. M. Ceperley, *Phys. Rev. B* **21**, 999 (1980). (b) P. A. Whitlock, D. M. Ceperley, G. V. Chester, and M. H. Kalos, *ibid.* **19**, 5598 (1979).

¹¹(a) D. M. Ceperley and M. H. Kalos, in *Monte Carlo Methods in Statistical Physics*, edited by K. Binder (Springer, Berlin, 1979), Chap. IV. (b) M. H. Kalos, D. Levesque, and L. Verlet, *Phys. Rev. A* **9**, 2178 (1974).

¹²R. A. Aziz, V. P. S. Nain, J. S. Carley, W. L. Taylor, and G. T. McConville, *J. Chem. Phys.* **70**, 4330 (1979).

¹³G. C. Maitland and E. B. Smith, *Chem. Phys. Lett.* **22**, 443 (1973).

¹⁴R. Ahlrichs, P. Penco, and G. Scoles, *Chem. Phys.* **19**, 119 (1976).

- ¹⁵D. R. McLaughlin and H. F. Schaefer, III, *Chem. Phys. Lett.* 12, 244 (1971).
- ¹⁶K. T. Tang, J. M. Norbeck, and P. R. Certain, *J. Chem. Phys.* 64, 3063 (1976).
- ¹⁷F. J. Pinski and C. E. Campbell, *Phys. Lett.* 79B, 23 (1978); F. J. Pinski (private communication); L. Whitney and C. E. Campbell (private communication).
- ¹⁸H. W. Jackson and E. Feenberg, *Ann. Phys. (N.Y.)* 15, 266 (1961).
- ¹⁹B. M. Axilrod and E. Teller, *J. Chem. Phys.* 11, 293 (1943); the coefficient is due to P. J. Leonard (unpublished), quoted by Ref. 1(b).
- ²⁰(a) P. R. Roach, J. B. Ketterson, and C. W. Woo, *Phys. Rev. A* 2, 543 (1970). (b) R. A. Aziz and R. K. Pathria, *ibid.* 7, 809 (1973).
- ²¹V. F. Sears, E. C. Svensson, A. D. B. Woods, and P. Martel, Atomic Energy of Canada Limited Report No. AECL-6779 (unpublished).
- ²²H. N. Robkoff, D. A. Ewen, and R. B. Hallock, *Phys. Rev. Lett.* 43, 2006 (1979).
- ²³E. C. Svensson, V. F. Sears, A. D. B. Woods, and P. Martel, *Phys. Rev. B* 21, 3638 (1980).
- ²⁴C. DeMichelis, G. L. Masserini, and L. Reatto, *Phys. Lett.* 66A, 484 (1978). A further description of the calculation is contained in G. Gaglione, G. L. Masserini, and L. Reatto, *Phys. Rev. B* 23, 1129 (1981).
- ²⁵P. M. Lam and G. C. Chang, *Phys. Lett.* 59A, 356 (1976).
- ²⁶F. W. Cummings, G. J. Hyland, and G. Rowlands, *Phys. Kondens. Mater.* 12, 90 (1970); G. J. Hyland, G. Rowlands, and F. W. Cummings, *Phys. Lett. A* 31, 465 (1970).
- ²⁷V. F. Sears and E. C. Svensson, *Phys. Rev. Lett.* 43, 2009 (1979); *Int. J. Quant. Chem.* 14, 715 (1980).
- ²⁸A. D. B. Woods and V. Sears, *Phys. Rev. Lett.* 39, 415 (1977).
- ²⁹D. O. Edwards and R. C. Pandorff, *Phys. Rev. A* 140, 816 (1965).
- ³⁰(a) D. S. Greywall, *Phys. Rev. A* 3, 2106 (1971). (b) J. F. Jarvis, D. Ramm, and H. Meyer, *Phys. Rev.* 170, 320 (1968).